Nanobody MET CAR-T cells show efficacy in solid tumors

Po-Han Chen[1], Qin Li[1], Sam Deveraux[2], Danielle K. Sohai[1], Pei-Chun Cha[1], Rianna Raghunandan[3], Nancy Chen[3], Yao Li[1], Mileena Nguyen[1], Michael C. Stankewich[1], Jon S. Morrow[1,4], Arnaud Augert[1,4], Qin Yan[1,4], and Samuel G. Katz[1,4,*]

Affiliations:

1. Department of Pathology, Yale School of Medicine, New Haven CT, USA
2. Division of Surgery and Interventional Science, University College London, London, UK
3. Yale College, Yale University, New Haven CT, USA
4. Yale Cancer Center, Yale School of Medicine, New Haven, CT, USA

Key words: MET, chimeric antigen receptor, immunotherapy, nanobody, mRNA

*Correspondence: Samuel.Katz@yale.edu

Samuel G. Katz, M.D., Ph.D.

Yale University School of Medicine

310 Cedar Street

Lauder Hall 315C

New Haven, CT 06520

Office: 203-785-2757

Fax: 203-785-3583

Abstract

Background: MET overexpression is associated with poor prognosis in many solid tumors due to its central role in tumor survival, invasion, metastasis, and chemoresistance. While targeting MET with antibody-drug conjugates has shown promising results, engineered cellular immunotherapeutic approaches have not been extensively explored. Compared to conventional single-chain variable fragments (scFv), naturally occurring single-domain antibodies consisting of variable heavy chains only (VHH or nanobodies) are smaller, retain high specificity, and exhibit remarkable biochemical stability. In this study, we tested the efficacy of MET-targeting VHH-CAR-T (chimeric antigen receptor T cells).

Methods: We generated a panel of VHH-CAR-Ts using mRNA electroporation. VHH-CAR-T cells were evaluated in functional assays including cell binding avidity, cytokine production profiles, hydrogel microwell-based cellular kinetics, and in vitro cytotoxicity. We also assessed the therapeutic efficacy of VHH-CAR-T in an in vivo mouse model of metastatic triple negative breast cancer (TNBC).

Results: Among the tested VHH, we identified those with intermediate avidity as most effective for in vitro tumor killing. VHH-CAR-Ts with CD28 costimulatory domains demonstrated augmented cytotoxicity with favorable selectivity, requiring a minimum antigen density threshold for activation. Mechanistically, VHH-CAR-Ts demonstrated low tonic signaling, high avidity, potent cytokine production, and rapid tumor killing kinetics. When administered in an mRNA format, VHH-CAR-Ts exhibited potent and prolonged control of tumor growth in an in vivo metastatic model of TNBC.

Conclusion: Taken together, these results demonstrate that VHH-CAR-Ts exhibit robust MET specificity and potent therapeutic efficacy both in vitro and in vivo. Thus, VHH-CAR-T cell therapy represents a promising immunotherapeutic strategy for targeting MET-overexpressing solid tumors.

What is already known on this topic: MET signaling is an important contributor to the aggressiveness of many solid tumors, and targeting MET by antibody-drug conjugates has shown efficacy and safety. Targeting MET by CAR-T cells has been under study, though with limited potency.

What this study adds: This study is the first to demonstrate effectiveness of anti-MET VHH-CAR-T cells. Compared with other antigen binding domains, VHH-incorporated CAR-T cells show low tonic signaling, a favorable cytokine profile, and potent tumor killing.

How this study might affect research, practice or policy: With the multiple advantages of VHHs including small size, stability, and low potential for tonic signaling, VHH-CAR-T cells represent a promising approach for CAR-T design against solid tumors.

INTRODUCTION

While chimeric antigen receptor (CAR) engineered T cells have shown impressive efficacy in hematologic malignancies, solid tumors pose many challenges. Target selection remains a challenge for solid tumors due to the lack of tumor-specific antigens[1]. Innovative CAR designs are also needed to promote tumor infiltration and persistence in the hostile tumor microenvironment, to overcome heterogeneous antigen expression, and to avoid on-target/off-tumor cytotoxicity.

The *MET* oncogene encodes the MET receptor tyrosine kinase, which is overexpressed in many solid tumors and is associated with poor prognosis due to its central role in mediating drug resistance and pro-survival signaling[2]. While tyrosine kinase inhibitors are available, their efficacy is limited to a select number of MET-addicted tumors with MET amplification or mutations[2]. In contrast, targeting MET expression with surface antibodies such as antibody-drug conjugates (ADCs) has shown safety and copy number/mutation-independent efficacy[3]. As CARs leverage the antigen recognition ability of antibodies with the additional benefits of adaptive T cell responses, targeting MET overexpression using CAR-T cells holds great potential.

The antigen recognition domain affects the target sensitivity, durability, and tonic signaling of CAR-T cells[4,5]. Most CARs use a single-chain variable fragment (scFv) as the antigen binding domain, which commonly exhibits self-clustering and tonic signaling leading to T cell exhaustion[6,7].

A variable region of a heavy-chain-only antibody (VHH or nanobody) is emerging as an alternative to scFv[8–10]. VHH-based CARs have been successfully used in BCMA-CAR-T cell therapy ciltacabtagene autoleucel (cilta-cel) against myeloma with approval from the U.S. Food and Drug Administration (FDA) [11]. Of particular importance for solid tumors, the stability of VHH helps avoid receptor clustering and tonic signaling; its uniquely long complementarity-determining region 3 (CDR3) enables targeting of cryptic epitopes and isoforms that may overcome tumor heterogeneity; its compact size allows flexible integration with other moieties (such as tandem VHH in cilta-cel) to facilitate innovative CAR designs with

97 enhanced functionality; finally, its high degree and ease of humanization reduce
98 immunogenicity and ensure safety in humans[8,11–15].
99 In this study, we constructed a panel of mRNA VHH-CAR-T cells targeting MET, and
100 demonstrate that VHH-CAR-T cells exhibit high avidity, potent cytokine production upon
101 stimulation, a potential therapeutic window for CAR activation, low tonic signaling, and
102 effective control of metastatic tumors in vivo – features that warrant further exploration as a
103 novel form of T cell immunotherapy for solid cancers.
104
105 **MATERIALS AND METHODS**
106 **Cells cultures:** Breast cancer cell line MDA-MB-231 was purchased from ATCC (HTB-26),
107 and its metastatic sub-population LM2 was a kind gift from J. Massagué. The non-small cell
108 lung cancer cell line A549 cell line was obtained from Peter Glazer, and the head and neck
109 squamous cell carcinoma cell lines FaDu and CAL27 cell lines were obtained from Barbara
110 Burtness. These cells were cultured in DMEM+10% FBS+1% penicillin/streptomycin. The
111 renal cancer cell line 786-O was obtained from Harriet Kluger and cultured in RPMI1640+10%
112 FBS+1% penicillin/streptomycin. The diffuse large B-cell lymphoma cell lines Karpas-422 and
113 OCI-LY3 were obtained from Markus Müschen and cultured in RPMI1640+20% FBS+1%
114 penicillin/streptomycin. Small-cell lung cancer cell lines NCI-H146 (ATCC HB173) and NCI-
115 H1341(ATCC CRL-5864) were cultured in DMEM-F12 supplemented with 10% FBS, 1X
116 Insulin-Transferrin-Selenium and 1% penicillin/streptomycin.
117
118 **Construction of CAR and *in vitro* transcription**: The CAR construct consists of a T7
119 promoter, 5'UTR (human beta-globin), CAR, P2A self-cleavable sequence, GFP, and 3'UTR
120 (human beta-globin) (see **Supplemental Figure 1A**). Binding domains for the nanobodies
121 (VHH1-5), 1E4 (scFv1) and 5D5 (scFv2) sequences were adapted from patents
122 WO2012/042026[16], US10116622B2[17] and US20190085063A1[18], respectively. The
123 scFv3 and NK1-CAR sequences were adapted from previous publications [19–21]. The CAR
124 sequences were synthesized as gene blocks containing T7 promoter and 5' and 3' UTR

125 sequences. They were cloned into standard pUC57 plasmid using the InFusion cloning kit
126 (Takara).
127 For *in vitro* transcription, a PCR product encompassing the T7 promoter and 3' UTR, where
128 the reverse primer also added a 100 nucleotide poly-A tail[22], was used in the T7 ARCA
129 HighScribe mRNA Kit with Tailing Reaction (NEB, Cat. #E6020S). Final mRNA was purified
130 using lithium chloride precipitation and concentrated to 1-2 μg/μL in water.
131
132 **Isolation and activation of primary human T cells:** Human peripheral blood mononuclear
133 cells were collected from healthy donors (either local draws under IRB protocol
134 HIC2000033275 or from the Gulf Coast Regional Blood Center). Bulk T cells were isolated
135 using the EasySep Human T Cell Enrichment Kit (STEMCELL Technologies, Cat. #17951),
136 activated with ImmunoCult Human CD3/CD2/CD28 T cell activator (STEMCELL, Cat. #10990)
137 at the recommended concentration, and cultured at 1 x 10^6 cells per mL in RPMI1640 + 10%
138 FBS in the presence of 100 IU/mL recombinant human IL-2 (Miltenyi Biotec, Cat. #130-
139 097743).
140
141 **Production of mRNA CAR-T cells:** On days 7-10 post T cell activation, T cells were pelleted,
142 washed, and resuspended in 20 μL MaxCyte buffer per 2 million cells. Electroporation was
143 performed using the MaxCyte ATX with the Expanded T cell Protocol 1 at 1 μg mRNA/1 million
144 T cells. Following electroporation, cells were rested in a 37^0C incubator with 5% CO_2 for 10
145 minutes and resuspended in complete T cell culture media at $2x10^6$ cells/mL with 100 IU/mL
146 IL-2. Cells were either frozen after 4 hours or used for experiments after overnight incubation.
147 Successful mRNA electroporation was confirmed by GFP expression using either
148 fluorescence microscopy or flow cytometry.
149
150 **Flow cytometry:** Immunophenotypes of all samples were analyzed using CytoFLEX S
151 (Beckman Coulter, CA, USA) flow cytometers. FlowJo software (Tree Star, OR, USA) was
152 used for data analysis. The following antibody-conjugated fluorophores were used: CD3

153 AlexaFlour 700 (1:100, clone OKT3, BioLegend 317340); CD8 BUV711 (1:100, clone RPA-
154 T8, BioLegend 301044); CD4 BUV605 (1:100, clone OKT4, BioLegend 317438); CD69
155 PE/Cy5 (1:100, clone FN50, BioLegend 310908); TNF-α PE (1:50, clone MAb11,BioLegend
156 502909); IFN-γ PerCP/Cy5.5 (1:100, clone XMG1.2, BioLegend 505822); IL-2 BV785 (1:50,
157 clone MQ1-17H12, BioLegend 500348); IL-4 PE/Dazzle 594 (1:100, clone MP4-25D2,
158 BioLegend 500832); PD-1 PE/Cy7 (clone A17188B, BioLegend 621616); TIM-3 APC (clone
159 A18087E, BioLegend 364804); LAG3 APC/Fire750 (clone 7H2C65, BioLegend 369214). MET
160 expression was confirmed by flow cytometry with a monoclonal anti-MET antibody (1:10,
161 Roche, clone SP44) compared to an IgG isotype control (BioLegend 400120).
162
163 **Gene expression database analysis:** Gene expression data for MET across human small
164 cell lung cancer (SCLC) cell lines were obtained from the SCLC-CellMiner database using the
165 SCLC Global response cell line set[23]. Z-scores corresponding to MET expression values
166 were extracted and visualized as a heatmap using GraphPad Prism to compare relative
167 expression levels across cell lines.
168
169 **Western blot:** Protein samples were resolved on 4–20% Mini-PROTEAN TGX precast
170 polyacrylamide gels (15-well, 15 µl; Bio-Rad, #4561096) and transferred to nitrocellulose
171 membranes. Membranes were blocked in 5% non-fat milk in Tris-Buffered Saline with 0.1%
172 Tween-20 (TBST) and incubated with primary antibodies overnight at 4°C (Beta-Actin, 1:5,000,
173 GTX629630; MET, 1:1,000, Cell Signaling Technology #4560). After washing, membranes
174 were incubated with HRP-conjugated secondary antibodies (1:3,000; Cell Signaling
175 Technology; anti-rabbit IgG #7074, anti-mouse IgG #7076) in 5% non-fat milk in TBST for 2
176 hours at room temperature. Blots were developed using an ultra-sensitive enhanced
177 chemiluminescent (Thermo Scientific, #34095) and imaged on Bio-Rad ChemiDoc imaging
178 system.
179

180 **Immunohistochemistry (IHC):** 4-μm sections were obtained from formalin-fixed, paraffin-
181 embedded (FFPE) tissue. Anti-MET antibody (clone SP44, AbCam, ab227637) was manually
182 applied at 1:50 dilution after antigen retrieval using Tris-EDTA buffer at pH 9.0. Anti-human
183 CD3 antibody (Biocare Medical, CP215) was applied at 1:75 dilution manually following
184 vendor protocol. IHC quantification was performed by visual examination of multiple high
185 power fields for % tumor positive for MET (all intensity).
186
187 **CD69 activation assay for CAR-Jurkat:** The protocol was similar to that previously described
188 [24]. Briefly, 30,000 target cells per well were plated in a 96-well plate. Jurkat cells were
189 electroporated with CAR mRNA and incubated at 37^0C for 4 hours before adding to target
190 cells at various E:T ratios (no target, 100:1, 10:1, 1:1). After overnight incubation, Jurkat cell
191 activation was measured by surface expression of CD69 using flow cytometry.
192
193 **In vitro tumor killing assays:** The flow-based killing assay was similar to that previously
194 described[25] with the following modification. Tumor cells labeled with 1 μM CellTrace Far
195 Red (Invitrogen C34572) were seeded in 24-well plates at a concentration of 1 x 10^5 cells/well.
196 Mock or CAR-T cells were added to the culture at different ratios (E:T of 0.5:1, 1:1, 2:1, 4:1)
197 without adding exogenous cytokines. Cells were analyzed 16 hours later to measure residual
198 tumor cells by flow cytometry. Dead cells were identified by Live/Dead Violet staining
199 (Invitrogen L34955). Tumor killing was calculated using the formula: % specific lysis = (1-#
200 residual target cells in treated group/# target cells cultured alone without T cells) x100%.
201 The luciferase-based killing assay was performed using cells expressing firefly luciferase
202 (MDA-MB-231, FaDu, and CAL27). Tumor cells were plated with CAR-T cells at the desired
203 E:T ratio in 384-well plates in 30 μL media overnight. Luminescence was detected using the
204 ONE-Glo Luciferase Assay System (Promega E6120) and analyzed using a plate reader
205 (BioTek, SYNERGYMx). Cell lysis (%) = (1 - (experimental readout - spontaneous
206 readout)/spontaneous readout) x 100.

207

208 **CellCyte tumor proliferation assay:** A lentiviral plasmid encoding mKate2 with puromycin
209 selection was obtained from Dr. David Fox at the University of Michigan. A549 tumor cells
210 expressing mKate2 were co-cultured with T cells in 96-well optically clear flat-bottomed plates
211 at an E:T ratio of 3:1. Plates were imaged using the CellCyte system (ECHO) every 4 hours,
212 and the number of mkate2-positive tumor cells was counted by the provided software.

213

214 **Mouse tumor xenograft:** Six-week-old female NOD.Cg-Prkdc^{scid} Il2rg^{tm1Wjl}/SzJ (NSG) mice
215 were purchased from the Jackson Laboratory (Strain #005557). Tumor inoculation was
216 performed via tail vein injection of $2x10^5$ cells in 100 μL PBS when the mice reached 9-10
217 weeks of age. Once injected tumors reached a total flux between 10^7 to 10^8 photons/sec by
218 bioluminescence imaging (BLI) (~7-10 days), mice were randomized into respective groups
219 and given weekly injections of PBS or T cells as specified in the text. To avoid graft-versus-
220 host disease, the day before each subsequent T cell injection, 60 mg/kg cyclophosphamide
221 was injected intraperitoneally to deplete the previously injected T cells [26]. Tumor burden was
222 monitored by weekly BLI using the Xenogen *In Vivo* Imaging System (IVIS) (Caliper Life
223 Sciences) and analyzed with Living Image software. Animals were euthanized once
224 luminescence signals reached $1x10^9$ photons/sec or when animals developed significant
225 stress.

226

227 **Cell force binding assay (avidity):** CAR-tumor binding force was measured using the z-Movi
228 device (LUMICKS, Amsterdam, The Netherlands). Target cells were seeded onto microfluidic
229 chips at a concentration of $5x10^7$ cells per mL to obtain a confluent monolayer. CAR-T cells
230 were labeled with 1 μM CellTrace Far Red to enable T cell tracking. After co-incubation of
231 CAR-T cells with the tumor monolayer for 2.5-5 minutes, a force ramp ranging from 0 to 1000
232 pN was applied for 2.5 minutes. T cell detachment was detected by fluorescence imaging. The
233 binding force was analyzed using the Oceon software (V.1.0, LUMICKS).

234

235 **Cytokine release assay:** For intracellular cytokine staining assays, T cells and target cells
236 were co-cultured at a 1:1 E:T ratio for 5-12 hours in the presence of 2 μM brefeldin A (BD
237 GolgiPlug, cat # 51-2301KZ). For the bulk cytokine assay, the supernatants from overnight
238 co-culture were harvested and stored in -20^{0}C before shipping to Eve Technologies.
239 For the multiplexed secretome assay, after stimulation with target cells, approximately
240 30,000 magnetically enriched CD8+ CAR-T cells were processed for membrane staining
241 (AF647-CD8, STAIN-1002-1). Subsequently, these cells were loaded onto the IsoCode chip
242 (IsoPlexis, ISOCODE-1001-4), comprising 12,000 chambers prepatterned with an array of 32
243 cytokine capture antibodies. The chip was then incubated in the IsoLight machine for 16 hours
244 at 37°C with 5% CO_2 supplementation. A cocktail of detection antibodies was then applied to
245 detect the secreted cytokines, followed by fluorescence labeling. The resulting fluorescence
246 signals were analyzed using IsoSpeak v.2.8.1.0 (IsoPlexis) to determine the number of
247 specific cytokine-secreting cells and the intensity level of each cytokine.
248

249 **Structural modeling:** The structures of the VHH sequences, scFv1 (1E4) and scFv2 (5D5),
250 and their respective complexes with the human MET extracellular domain were predicted
251 using AlphaFold3[27]. Antibody-MET affinity was estimated using the HADDOCK PRODIGY
252 server [28,29]. Structural modeling and analysis were performed using PyMOL (Schrödinger,
253 LLC).
254

255 **Microwell co-culture system:** We used the TROVO system (Enrich Biosystems) for the
256 microwell assays. For the tumor killing and T cell proliferation assay, T cells (stained with
257 CD4/CD8-Alexa647) and MDA-MB-231 cells were plated at a 2:1 effector to target ratio in a
258 six-well culture plate, with each well containing 3,200 printed hydrogel microwells. Each
259 microwell was indexed by proprietary software and imaged every 12 hours over a four-day
260 period for downstream analysis. Tumor killing was defined as a ≥15% reduction in tumor area
261 compared to day 0. T cell proliferation was defined as a ≥2-fold increase in stained T cell area

262 compared to day 0. For the single cell killing assay, CAR-T cells and tumor cells were plated
263 at a 1:10 E:T ratio, and only microwells containing a single T cell were selected for further
264 imaging analysis. The percentages of microwells with tumor killing/T cell proliferation, and rate
265 of killing were calculated by the proprietary software built into the TROVO system.

266 In detail, percentage of microwells with tumor killing or T cell proliferation is calculated as
267 number of microwells meeting the killing/proliferation threshold stated above divided by total
268 number of microwells in this well. Bar graph is average +/- standard deviation of 3 technical
269 replicate wells.

270 Single cell killing rate was estimated by fitting the paired T cell and tumor signals (area or
271 counts) at each time point to a mass-action interaction model. For each CAR-T construct (and
272 matched controls), we ran three independent 3,200-well microwell plates (9,600 wells/clone
273 total). Dilute seeding targeted ~1 T cell and ~10 tumor cells per well. Plates were imaged from
274 0–96 h; fluorescence at time zero was used to calibrate area-to-cell conversions. Tumor-only
275 wells on the same plates were fit to an exponential model $C(t) = C_0e^{[rC\cdot t]}$ to estimate the
276 plate-level tumor growth rate rC. From the full set, we retained ~800–900 co-culture wells per
277 sample that met pre-specified QC (confirmed single T at time zero, adequate tumor baseline,
278 stable focus/tracking, and finite parameter estimates). An effective killing rate (k_eff) was then
279 obtained per well using a simplified Lotka–Volterra–type predator–prey coupling $dC/dt = rC\cdot C$
280 $- k_eff\cdot T\cdot C$ (classical LV prey equation) and the same mass-action kill term described in
281 similar CAR-T models[30], i.e., tumor loss regressed against cumulative T cell exposure. Fits
282 were performed by nonlinear least squares with plate-specific rC; Fitting results with
283 goodness-of-fit $R^2 > 0.95$ are included. For each CAR-T construct, the distribution of k_eff was
284 summarized per plate, and the construct-level average k_eff and standard deviation was
285 calculated across the triplicated experiments.

286

287 **Statistics:** All statistical analyses were conducted using Prism v.10 (GraphPad). Unless
288 otherwise specified, data were presented as mean ± SD. Statistical significance was

289 determined by paired t-test, one-way analysis of variance (ANOVA), or two-way ANOVA as
290 indicated in the figure legends. The log-rank (Mantel-Cox) test was used to determine
291 statistical significance for overall survival in mouse experiments.
292
293 **RESULTS**
294 **VHH-CAR-T with intermediate avidity showed the most potent tumor killing**
295 We curated five camelid-derived VHH nanobody sequences and incorporated them into a
296 second-generation mRNA CAR design with a CD8 hinge and transmembrane domain,
297 followed by 4-1BB and CD3ζ signaling domains (**Supplemental Figure 1 and Figure 1A**).
298 Since avidity represents the strength of the immune synapse and has been shown to
299 predict clinical response[31], we used the z-Movi system to measure the avidity of different
300 VHH-CAR-T cells. To ensure that avidity measurement was not confounded by different CAR
301 expression levels, the amount of electroporated mRNA was adjusted so that all constructs
302 had >85% expression as determined by GFP; however, VHH5-CAR was consistently
303 expressed at ~75-80% regardless of amount of mRNA input (**Figure 1B**).
304 All VHH-CAR-Ts showed varying percentages of bound T cells with increasing rupture
305 force (**Figure 1C**). VHH1, VHH2, and VHH3 showed relatively low avidity compared to VHH4
306 and VHH5. Despite lower expression, VHH5 surprisingly showed the highest avidity. The
307 mean percentage of remaining T cells bound to targets at 1000 pN, from the lowest to highest,
308 was VHH3 (7%), VHH1 (12%), VHH2(19%), VHH4 (31%), and VHH5 (36%) (**Figure 1D**).
309 To gain structural insight into functional avidity, we modeled the binding of the different
310 VHHs to MET using AlphaFold3 (**Figure 1E**). VHH1, VHH2, and VHH5 are predicted to
311 overlap with the high affinity binding site for the HGF-α chain. VHH3 is predicted to bind to a
312 more membrane-distal epitope that overlaps with HGF-β chain. VHH4 appears to bind to a
313 distinct epitope separate from the other VHHs, slightly away from either HGF binding site.
314 These predictions are consistent with the reported antagonistic effect of these VHHs on the
315 HGF-MET interaction. The dissociation constant K_D was estimated by PRODIGY for the top-
316 ranked structures. The affinity for VHH3 ranged from ~10-50 nM; VHH1 and VHH2 showed

317 intermediate affinity, averaging 5-10 nM; VHH4 and VHH5 had the highest affinity, ranging
318 from 0.4-1.2 and 2-3 nM, respectively. The estimated affinities correlated with the observed
319 avidity, suggesting a direct relationship between affinity and immune synapse strength.
320 We then investigated whether different avidities correlate with the in vitro cytotoxic
321 functions of effector cells, expecting higher avidity to achieve better killing of MDA-MB-231
322 cells. Surprisingly, we found that lower avidity CARs mediated stronger tumor killing, with
323 VHH1 and VHH2 achieving the highest level of cytotoxicity (**Figure 1F**). VHH3 showed the
324 lowest avidity, but achieved slightly better killing than VHH4 and VHH5. The superior tumor
325 killing by VHH1, VHH2, and VHH3 was most notable at low E:T ratios. There was no significant
326 difference in cytotoxicity between VHH1 and VHH2. Consistently, we showed that both VHH1
327 and VHH2 strongly inhibit proliferation of A549 lung cancer cells over a 70-hr period using the
328 CellCyte system (**Figure 1G**).
329 Although high-avidity CARs are generally favored and have been shown to correlate with
330 clinical response, our findings are consistent with emerging evidence documenting potential
331 advantages of lower-avidity CARs (see Discussion). Given that there was no significant
332 difference between VHH1 and VHH2 in terms of avidity and in vitro cytotoxicity, we used VHH2
333 for further characterization.
334
335 **CD28 costimulatory domain conferred stronger VHH-CAR-T activation than 4-1BB**
336 Using VHH2, we next investigated how different cytoplasmic costimulatory domains,
337 namely, CD28 versus 4-1BB, affect VHH-CAR-T function.
338 Although not significantly different, VHH2-28z trends towards higher avidity than VHH2-
339 BBz (**Figures 2A and B**). VHH2-28z also achieved higher in vitro tumor killing and more
340 immune cytokine (IFN-γ, TNF-α, IL-2, and IL-4) and cytotoxic molecule Granzyme B
341 production, as well as higher polyfunctionality (**Figures 2C-E, and Supplemental Figure 2**).
342 In addition to these fixed-time point assays, we also used a microwell-based co-culture
343 platform to gain insights into the kinetics of CAR-T cell killing. In microwells where we seeded
344 1 effector T cell per 10 tumor cells (1:10 E:T), we found that VHH2-28z demonstrated a higher

345 single-cell killing rate than VHH2-BBz (**Figure 2F**). At an experimental setup of a 20:10 E:T
346 ratio, we observed more tumor killing and higher T cell proliferation associated with VHH2-28z
347 compared to VHH2-BBz over a four-day period (**Figures 2G-I**). Although CD28 costimulatory
348 domain confers immediate potency, it is reported to be more prone to exhaustion than 4-
349 1BB[32]. However, most likely due to the transient nature of mRNA CAR expression, we did
350 not observe significant increase in exhaustion markers PD-1, LAG3, or PD-1+/TIM3+ for
351 VHH2-28z (**Supplemental Figure 3**).Our data is consistent with higher and more rapid
352 cytotoxic function generally reported for CD28 compared to 4-1BB[32,33]. Beyond four days,
353 most likely due to diminishing mRNA, there was no significant killing or proliferation observed
354 with either construct (data not shown). In subsequent studies, we used VHH2-28z unless
355 otherwise specified.
356
357 **VHH2-CAR-T eliminated MET+ tumor cells in vitro and in vivo**
358 Since MET overexpression is associated with poor prognosis in many solid tumors, we
359 tested the efficacy of VHH2-CAR-T against different subtypes of solid tumors with known MET
360 overexpression. VHH2-CAR-T demonstrated cytotoxicity against tumor cell lines from TNBC
361 (MDA-MB-231 and LM2), clear cell renal cell carcinoma (786-O), and head and neck
362 squamous cell carcinoma (CAL27 and FaDu) (**Figures 3A and B**).
363 Recent clinical trials have shown that repeated CAR-T cell injections exert better tumor
364 control than single CAR-T administration in solid tumors[34,35]; presumably because fresh
365 supplies of T cells help overcome T cell exhaustion in the tumor microenvironment [34]. We
366 tested the in vivo efficacy through weekly injections of fresh mRNA VHH2-CAR-T cells (**Figure**
367 **3C**). We focused on the aggressive lung metastatic TNBC model LM2. Luciferase-expressing
368 LM2 tumor cells were injected intravenously (IV) via the tail vein into NSG mice. After 7-10
369 days, we confirmed tumor growth in bilateral lungs by bioluminescence imaging (BLI). We
370 then injected PBS, $20x10^6$ mRNA VHH2-CAR-T cells or an equal number of mock T cells via
371 the tail vein, followed by three additional weekly injections of $5x10^6$ effector cells or PBS.

372 Significant reduction in tumor growth was observed in the VHH2-CAR-T group compared
373 to the mock T cell group (**Figure 3D**). Mice were euthanized on day 25 for necropsy.
374 Immunohistochemical (IHC) staining with anti-MET revealed heterogeneous MET expression
375 within the tumor bed in the mock T cell and PBS groups (**Figure 3E**). Although some residual
376 tumor cells were seen in the VHH2-CAR-T group, they were mostly MET negative by IHC
377 (**Figure 3E**); the tumor growth curve also suggested slow growth of these residual tumors
378 (**Figure 3D**). In the VHH2-CAR-T group, IHC for human CD3 showed clear infiltration and
379 aggregation of T cells in the residual tumors, whereas the mock T cell group showed only
380 limited numbers of single scattered T cells (**Figure 3F**). Given the aggressive nature of tumors
381 generally associated with MET overexpression, these findings indicate that VHH2-CAR-T
382 could efficiently control tumor growth by eliminating MET-positive tumor cells.
383
384 **VHH2-CAR-T activity is dependent on MET expression level**
385 Given the necropsy findings that MET can be expressed at heterogenous levels in different
386 tumor cells, we next tested the antigen threshold for VHH2-CAR-T activation. First, in a panel
387 of small cell lung cancer cell lines with varying levels of MET expression[23] (**Figure 4A**), we
388 observed that increased MET expression resulted in increased cytotoxicity by VHH2-CAR-T,
389 indicating that targeted tumor lysis was dependent on MET expression level (**Figure 4B-E**).
390 To further investigate antigen-dependent cytotoxicity, we compiled and analyzed a series
391 of cell lines with varying levels of MET expression and tested cytotoxicity at a high E:T ratio of
392 5:1 (**Figure 4F-G**). As expected, co-culture of VHH2-CAR-T with cell lines with high levels of
393 MET expression (786-O, NCIH1341, LM2, and Karpas-422) led to significant tumor cell death
394 ranging from 80-100%. Although the intermediate MET-expressing cell line, NCIH146, still
395 showed significant cell death, the killing by VHH2-CAR-T dropped to approximately 45-50%
396 (against a background of ~10% mock T cell killing). For the low-MET cell line, OCI-LY3, and
397 MET-negative cell line, K562, VHH2-CAR-T showed cytotoxicity not significantly different from
398 mock T cells.

399 Taken together, our findings suggest the existence of an antigen threshold level for VHH2-
400 CAR-T activity. In normal tissues, MET is expressed at the highest level in hepatocytes, whose
401 MET expression level is predicted to fall between OCI-LY3 and K562 cell lines, for which we
402 observed limited cytotoxicity and a potential therapeutic window for VHH2-CAR-T cells.
403
404 **VHH-CAR-T cells showed low tonic signaling**
405 Since nanobodies generally show high stability[8,12], we tested how incorporation of VHH
406 influences CAR-T cell function compared to MET-CAR-T cells engineered with different
407 sources of antigen binding domains (ABDs).
408 To facilitate comparison, we adapted a previously reported CAR-Jurkat (CAR-J) assay [24]
409 (**Figure 5A**). We electroporated mRNA encoding CARs with various ABDs into Jurkat cells,
410 co-cultured them with tumor cell lines at various effector to target ratios for 16 hours, and
411 assessed expression of CD69 activation marker by flow cytometry. The diffuse large B-cell
412 lymphoma (DLBCL) cell line, Karpas-422, served as a convenient target for this assay as it
413 expresses high levels of CD19 in addition to MET, thus allowing comparison with CD19-CAR
414 (FMC63) as a positive control (**Supplemental Figure 3**).
415 The selected ABD constructs included three different scFvs, one natural ligand, and VHH1-
416 4 (**Figure 5B**). ScFv1 and scFv3-CAR-J were constructed similarly to previously described
417 cell lines [19,20]; scFv2-CAR-J was derived from the monoclonal antibody Onartuzumab
418 (5D5)[36]. Finally, a natural ligand CAR previously shown to mediate cytotoxicity against
419 mesothelioma was derived from the NK1 domain of HGF[21].
420 As expected, CD19-CAR-J cells showed an antigen-dependent increase in CD69
421 expression, whereas mock Jurkat cells showed only basal levels of expression at all E:T ratios
422 (**Figure 5B**). The tested scFv-CAR-J cells, however, demonstrated a wide range of antigen-
423 dependent responses. Notably, scFv1-CARJ showed high basal levels of CD69 expression in
424 the absence of Karpas-422, indicating tonic signaling. Indeed, increasing the target cell ratio
425 did not lead to a further increase in CD69 expression, suggesting T cell dysfunction. In contrast,
426 scFv2-CAR-J showed low basal levels and an antigen-dependent increase in CD69. scFv3-

427 CAR-J showed low basal CD69 levels, but for an unknown reason did not show an antigen-
428 dependent response. The ligand-based NK1-CAR-J also failed to show significant CD69
429 expression upon stimulation. In contrast to the varied behaviors of the tested scFv- and ligand-
430 CAR-J cells, all VHH-CAR-J cells demonstrated low basal levels and an antigen-dependent
431 increase in CD69 expression. The various tonic signaling profiles seen in Jurkat cells could
432 be replicated in co-cultures of primary human T cells and MDA-MB-231 target cells (**Figure**
433 **5C**).

434 To further show that tonic signaling leads to T cell dysfunction, we chose the tonic scFv1
435 and the low-tonic scFv2 and VHH2 for comparison. As expected, scFv1-CAR-T cells showed
436 only limited tumor killing compared to scFv2- and VHH2-CAR-T cells, both of which showed
437 equivalent tumor killing at various E:T ratios (**Figure 5D and 5E**).

438 The predisposition of different ABDs for tonic signaling is intriguing. Because previous
439 reports have correlated positive surface charges of ABDs with tonic signaling[37], we modeled
440 the electrostatic surfaces for scFv1, scFv2, and VHH2 (**Figure 5F**). However, structural
441 modeling showed no obvious differences in net surface charges, suggesting that other
442 mechanisms might contribute to tonic signaling (see Discussion).

443

444 **Different binders endowed varying functional profiles to CAR**

445 We further tested whether low tonic signaling of VHH affects avidity, cytokine secretion,
446 and tumor killing kinetics. Again, we compared VHH2 with scFv1 and scFv2. All three appear
447 to share similar predicted affinities (5-10 nM). However, structural modeling predicts different
448 binding epitopes on MET; while VHH2 and scFv1 occupy a more membrane-proximal epitope,
449 scFv2 binds to a more membrane-distal one (**Figure 6A**).

450 We first compared how the three ABDs influence avidity, expecting roughly equal avidity
451 given their equivalent affinities. Interestingly, despite similar expression levels of all constructs
452 (**Figure 6B**), VHH2 consistently showed stronger avidity than scFv2, which was greater than
453 scFv1 for two different tumor cell lines (**Figures 6C-D**). The low avidity of scFv1 could be
454 related to factors that also contributed to its tonic signaling. The stronger avidity of VHH2 over

455 scFv2 was unclear, but one possible explanation could be related to VHH2's binding to a more
456 membrane-proximal epitope, as targeting membrane-proximal epitopes has been shown to
457 stabilize the immune synapse[38,39].

458 In terms of cytokine production, both scFv2 and VHH2 showed higher levels of IFN-γ, TNF-
459 α, and IL-2 after target stimulation than scFv1 (**Figure 6E** and **Supplemental Figure 4**).
460 Among the three constructs, scFv2 was noted to have the highest baseline cytokine secretion
461 in the absence of antigens (especially IFN-γ), suggesting some tonic signaling in scFv2. Using
462 IsoPlexis, VHH2 demonstrated the highest polyfunctional strength index (PSI) in vitro (**Figure**
463 **6F**), including the highest effector, stimulatory, and chemoattractive and lower regulatory
464 cytokine levels. Although there were increased inflammatory cytokines detected by IsoPlexis
465 for VHH2, by ELISA VHH2 produced lower levels of proinflammatory cytokines such as IL-6,
466 IL-8, IL-10, IL-1β, and granzyme A (**Supplemental Figure 4**). The reason for this difference
467 is unclear but might be due to different assay conditions.

468 We also examined the kinetics of tumor cell killing using a microwell platform monitored
469 over four days (as in Figure 2F-I). Although not statistically significant, VHH2-CAR-T cells
470 trended to have the highest single-cell killing rate (**Figure 6G**), the highest percentage of
471 microwells with tumor killing (**Figure 6H**), as well as the highest T cell proliferation (**Figure 6I**).
472 Taken together, these data suggest diverse behaviors of different MET-CAR-T cells, and that
473 VHH2-CAR-T cells have high avidity, potent immune cytokine production including
474 polyfunctionality, and rapid tumor killing kinetics.

475

476 **VHH2-CAR-T showed potent in vivo efficacy in comparison with scFv2-CAR-T**

477 Emerging evidence suggests that avidity correlates with in vivo and clinical efficacy more
478 so than in vitro cytotoxicity[31]. We tested this hypothesis by comparing VHH2 and scFv2 in
479 vivo given their overall similar in vitro cytotoxicity but differing avidities. Since multiple high
480 doses of VHH2-CAR-T cells appeared to provide potent tumor control (**Figure 3**), we

481 performed a CAR-T cell stress test by reducing the weekly dose to $2x10^6$ CAR-T cells per IV
482 injection and monitored tumor growth over a longer time period (**Figure 7A**).
483 Both VHH2-CAR-T and scFv2-CAR-T groups showed significantly better survival than
484 mock T cells and PBS, and VHH2-CAR-T conferred slightly longer survival than scFv2-CAR-
485 T (close to statistical significance) (**Figures 7B-D**). There was a significant reduction in tumor
486 growth rate in the VHH2 and scFv2 groups compared to saline or mock T cells (**Figures 7C-**
487 **D**). Interestingly, after the last CAR-T cell injection at day 21, many animals in the VHH2 group
488 showed lower tumor burdens than the scFv2 group. Three animals in the VHH2 group showed
489 continuous tumor control until approximately day 67. Overall, there were also fewer
490 extrapulmonary metastases in the surviving mice in the VHH2 group compared to the scFv2
491 group (**Figure 7D**). Collectively, our in vivo model indicates that VHH2-CAR-T cells are as
492 effective as scFv2-CAR-T cells with modestly enhanced tumor control, likely due to more
493 complete elimination of MET-positive tumor cells by the stronger avidity VHH2.
494 Although there was no overall survival difference between VHH2- and scFv2-CAR-T cells,
495 some of the mice appeared to die due to factors other than tumor burden thus complicating
496 survival curve analysis. On-target/off-tumor cytotoxicity (OTOT) was unlikely as the VHH2
497 does not bind murine MET[40], and histology showed no obvious evidence of tissue damage.
498 Other etiologies including cytokine storm or development of early GVHD were also possible.
499

500 **DISCUSSION**

501 We used an array of functional assays to comprehensively characterize nanobody-based
502 CAR-T against MET-positive solid tumors. Among a panel of VHH, we found that VHH1 and
503 VHH2 with intermediate avidity mediated the best killing especially at low E:T ratios. The CD28
504 costimulatory domain enhanced VHH2-CAR-T cell in vitro cytotoxicity and effectively
505 controlled tumor growth in vivo. Despite their potency, VHH2-CAR-T cells displayed an
506 antigen threshold that could potentially discriminate between tumor and normal tissues.
507 Compared to the more variable behaviors of scFv-CAR-T cells, VHH-CAR-T cells showed low
508 tonic signaling, high avidity, a favorable cytokine profile, and rapid tumor killing kinetics -

509 features that likely contributed to prolonged tumor control in vivo despite the transient nature
510 of the injected mRNA CAR-T cells.

511 This study highlights construct design as a crucial step in optimizing CARs. We examined
512 the fundamental aspects of changing the ABD with VHH as a comparison to scFv or ligand-
513 based approaches. Nanobodies are known for their small size and high stability [8–10]. We
514 demonstrated that all our tested VHHs have low tonic signaling, whereas the selected scFv
515 were more variable, with scFv1 being the most prominent example of a tonic signaling CAR.
516 Interestingly, structural modeling of scFv1 did not indicate excessive surface positive charges
517 that were previously reported to increase tonic signaling potential[37]. However, other
518 mechanisms, such as hydrophobic interactions and light-chain-heavy-chain mispairing are
519 also known to occur in scFv and might contribute to the tonic signaling of scFv1[5]. Although
520 not without limitations (such as the need for humanization), VHHs might generally offer an
521 alternative solution for some tonic signaling CARs [4].

522 We found that the two intermediate avidity VHH1 and VHH2 were more efficacious at
523 eliminating tumors than either the higher avidity VHH4/VHH5 or the lower avidity VHH3. There
524 is a complicated relationship between avidity and cytotoxicity—some prior publications
525 suggest that increased avidity leads to better CAR-T cell performance[41,42], while others
526 indicate that decreased avidity is preferable[38,43]. One potential explanation is that CAR-T
527 cells with high avidity have low *Koff* and therefore prolonged engagement with tumor cells,
528 which can lead to activation-induced cell death and compromised tumor killing[38,43]; on the
529 other hand, excessively low avidity translates to an unstable immune synapse. In another
530 context, VHH2-28z showed a trend toward higher avidity and cytotoxic function than VHH2-
531 BBz, likely due to the predisposition of CD28 to dimerize and thus promote multivalent
532 interactions[32,44,45]. Finally, the higher avidity of VHH2 compared to scFv2 could potentially
533 be related to VHH2's binding to a more membrane-proximal epitope and correlated with
534 slightly better tumor killing kinetics and tumor control in vivo. These findings reflect the
535 multifactorial nature of avidity, which depends on CAR-target antigen affinity, binding valency,

536 and CAR-antigen orientation, among other factors. Future studies will benefit from a better
537 understanding of the factors that influence the avidity-CAR function relationship.

538 Although the CD28 costimulatory domain led to higher and faster killing as shown here,
539 other studies have demonstrated earlier T cell exhaustion than 4-1BB[32]. However, we did
540 not observe notable differences in PD-1 and LAG3 expression between VHH2-28z versus
541 VHH2-BBz, perhaps due to short duration of mRNA CAR expression. For targeting solid
542 tumors, it might be advantageous to couple CARs with the CD28 costimulatory domain in an
543 mRNA format to achieve immediate and maximal tumor killing without the development of T
544 cell exhaustion, as outlined in a recent review[34].

545 VHH2-CAR-T cells appeared to have an antigen threshold for activation and thus a
546 possible therapeutic window. Encouragingly, a phase 1 trial of a MET CAR using the same
547 scFv2 (5D5) demonstrated safety with mostly clinically manageable grade 1-2 cytokine
548 release syndrome (CRS)[46]. Given that CAR-T cells generally require a high number of target
549 antigens to be present to become activated, therapeutic windows are likely present between
550 normal tissues and MET-overexpressed tumors, as shown here and illustrated elsewhere[47].
551 One future direction includes exploring logic-gated CAR design to further minimize on-
552 target/off-tumor toxicity.

553 Despite the short duration of our mRNA CARs, some VHH2-treated mice displayed
554 remarkably prolonged tumor control until day 67, even after cessation of CAR-T cell injections
555 on day 21. This prolonged tumor control was likely due to the ability of the high avidity and
556 polyfunctional VHH2-CAR-T cells to kill most of the MET-positive cells, which were
557 presumably more proliferative than the MET-negative cells within the same tumor. One can
558 imagine a future strategy against solid tumors that would deploy potent effector like VHH2-
559 CAR-T cells to target a surface antigen related to tumor aggressiveness (e.g. MET) to achieve
560 prolonged tumor control before bridging to other therapies.

561 The use of mRNA in the current study offered many advantages but also some limitations.
562 The main advantages included uniform CAR expression and high T cell viability, which
563 facilitated construct comparisons in multiple assays. Looking forward, mRNA represents a

564 particularly promising platform for CAR-T cell reprogramming given the current progress in
565 developing in vivo nanoparticle delivery systems[48]. However, in some experiments, such as
566 the microwell co-culture and xenograft mouse models, it would have been beneficial to use a
567 persistent CAR system so that one could monitor long-term tumor control and T cell functions.
568 In summary, we have shown the efficacy of a novel class of VHH-CAR-T cells against MET
569 with promising in vitro attributes as well as strong tumor control in vivo. The VHH-CAR-T cell
570 system warrants further preclinical study and development, including VHH humanization and
571 further construct optimization.
572
573 **Declarations:**
574 **Data availability statement:** All data relevant to the study are included in the article or
575 uploaded as supplementary information.
576 **Ethics statements**: Patient consent for publication: Not applicable.
577 **Ethics approval:** This study did not include human subjects. All animal studies were
578 approved by the Yale Institutional Animal Care and Use Committee.
579 **Funding:** This work was supported by National Institutes of Health (NIH) grants
580 R21CA263437 and R21CA282629, Department of the Army award ME220220, a
581 Developmental Research Program Grant from the Yale Head and Neck SPORE, P50
582 DE030707, Public Health Service grant number P50CA302572 from the University of Iowa
583 Neuroendocrine Tumor Specialized Program of Research Excellence and the National Cancer
584 Institute, and the CT Breast Health Initiative grant to S.G.K., Lion Heart Breast Cancer Pilot
585 Grant from Yale Cancer Center and Yale Cancer Center Immuno-Oncology K12 training grant
586 K12CA215110 to P-H.C., and NIH grant R01CA237586, Deparatment of Defense Breast
587 Cancer Research Program Award HT9425-23-1-0602 and CT Breast Health Initiative grant to
588 Q.Y. Work carried out by S.D. was supported by the UKRI Medical Research Council
589 [MR/W006774/1]. D.K.S was supported by the Yale School of Medicine immunohematology

590 T32 training grant 5T32HL007974-24. Funders had no involvement in study design, data
591 collection, data analysis, data interpretation, manuscript writing, or the decision to submit.

592 **Conflict of Interest:** P-H.C. and S.G.K. have a patent pending on the MET CAR.

593 **Author contributions:** P-H.C. and S.G.K. designed all the experiments and wrote the
594 manuscript. P-H.C. designed and performed all the experiments. Q.L., S.D., D.K.S., and P-
595 C.C. contributed to data figures and experiments. R.R. and N.C. contributed to molecular
596 biology and cloning of different CAR constructs. M.N. and A.A. contributed cell lines and
597 performed western blot and mRNA analysis. Y.L. and Q.Y. helped design and perform the *in*
598 *vivo* experiment. All authors reviewed the manuscript.

599 **Acknowledgments:** The research was performed as part of the Yale Pathology Physician-
600 Scientist training track. We also appreciate the support from the K12 Yale Immuno-Oncology
601 Training Program at Yale Cancer Center. We thank the Yale Animal Research Facility, for
602 excellent technical support. We also thank the Yale Flow Cytometry Core Facility for
603 maintaining and making available the cytometers used in the research. The Core is supported
604 in part by an NCI Cancer Center Support Grant # NIH P30 CA016359. We also thank Keck
605 Microarray Shared Resource (KMSR) at Yale University for providing the necessary services
606 using the IsoSpark system, which is funded in part by the National Institutes of Health
607 instrument grant 1S10OD034429-01.

608

609 **REFERENCES:**

610 1. Kembuan GJ, Kim JY, Maus MV, Jan M. Targeting solid tumor antigens with chimeric
611 receptors: cancer biology meets synthetic immunology. Trends Cancer. 2024;10:312–31.
612 https://doi.org/10.1016/j.trecan.2024.01.003

613 2. Comoglio PM, Trusolino L, Boccaccio C. Known and novel roles of the MET oncogene in
614 cancer: a coherent approach to targeted therapy. Nat Rev Cancer. Nature Publishing Group;
615 2018;18:341–58. https://doi.org/10.1038/s41568-018-0002-y

616 3. Wang J, Anderson MG, Oleksijew A, Vaidya KS, Boghaert ER, Tucker L, et al. ABBV-
617 399, a c-Met Antibody-Drug Conjugate that Targets Both MET-Amplified and c-Met-
618 Overexpressing Tumors, Irrespective of MET Pathway Dependence. Clin Cancer Res Off J
619 Am Assoc Cancer Res. 2017;23:992–1000. https://doi.org/10.1158/1078-0432.CCR-16-1568

620 4. Shukla D, Gabunia K, McGettigan SE, Patel PR, Christensen S, Fan T-J, et al. CAR
621 Binders Affect CAR T-cell Tonic Signaling, Durability, and Sensitivity to Target. CANCER
622 Immunol Res.

623 5. Ajina A, Maher J. Strategies to Address Chimeric Antigen Receptor Tonic Signaling. Mol
624 Cancer Ther. 2018;17:1795–815. https://doi.org/10.1158/1535-7163.MCT-17-1097

625 6. Frigault MJ, Lee J, Basil MC, Carpenito C, Motohashi S, Scholler J, et al. Identification of
626 Chimeric Antigen Receptors That Mediate Constitutive or Inducible Proliferation of T Cells.
627 Cancer Immunol Res. American Association for Cancer Research; 2015;3:356–67.
628 https://doi.org/10.1158/2326-6066.CIR-14-0186

629 7. Minguet S, Maus MV, Schamel WW. From TCR fundamental research to innovative
630 chimeric antigen receptor design. Nat Rev Immunol. 2025;25:212–24.
631 https://doi.org/10.1038/s41577-024-01093-7

632 8. De Meyer T, Muyldermans S, Depicker A. Nanobody-based products as research and
633 diagnostic tools. Trends Biotechnol. 2014;32:263–70.
634 https://doi.org/10.1016/j.tibtech.2014.03.001

635 9. Vincke C, Loris R, Saerens D, Martinez-Rodriguez S, Muyldermans S, Conrath K. General
636 strategy to humanize a camelid single-domain antibody and identification of a universal
637 humanized nanobody scaffold. J Biol Chem. 2009;284:3273–84.
638 https://doi.org/10.1074/jbc.M806889200

639 10. Ditlev SB, Florea R, Nielsen MA, Theander TG, Magez S, Boeuf P, et al. Utilizing
640 nanobody technology to target non-immunodominant domains of VAR2CSA. PloS One.
641 2014;9:e84981. https://doi.org/10.1371/journal.pone.0084981

642 11. Sun Y, Yang X-N, Yang S-S, Lyu Y-Z, Zhang B, Liu K-W, et al. Antigen-induced
643 chimeric antigen receptor multimerization amplifies on-tumor cytotoxicity. Signal Transduct
644 Target Ther. 2023;8:445. https://doi.org/10.1038/s41392-023-01686-z

645 12. Eisa AR, Tavassoli Razavi F, Hoseinzadeh A, Haghmorad D, Baharlou R. Nanobody
646 CAR-T cells in cancer: From molecular design to clinical translation. Biomed Pharmacother.
647 2025;193:118819. https://doi.org/10.1016/j.biopha.2025.118819

648 13. Blueggel M, Gül D, Stauber RH, Knauer SK. Small but mighty: the versatility of
649 nanobodies in modern medicine. Nanoscale Horiz. 2025;10:2158–71.
650 https://doi.org/10.1039/D5NH00283D

651 14. Lou H, Cao X. Antibody variable region engineering for improving cancer
652 immunotherapy. Cancer Commun. 2022;42:804–27. https://doi.org/10.1002/cac2.12330

653 15. Zhang XG, Wang L, Yang J, Hu XN, Wang H, Zhang LN, et al. Efficacy and safety of
654 BCMA nanobody CAR T-cell therapy in relapsed or refractory plasma cell myeloma. Blood
655 Adv. 2025;9:4543–52. https://doi.org/10.1182/bloodadvances.2025016322

656 16. Beste G, Denayer T, Hermans G, Szyroki A, Steffensen S, Ververken CJN. Biological
657 Materials Related to C-Met [Internet]. 2012 [cited 2026 Jan 4].
658 https://patentscope.wipo.int/search/en/WO2012042026. Accessed 4 Jan 2026

659 17. Yoo J, Nam JR, Yoo JS, Kim S-W, Lee WS, Shim SR, et al. Human antibody specific to
660 c-Met and preparation method thereof [Internet]. 2018 [cited 2026 Jan 4].
661 https://patents.google.com/patent/US10106622B2/en. Accessed 4 Jan 2026

662 18. Frigault MJ, Zhao Y, Scholler J, June CH. Compositions and Methods for Generating a
663 Persisting Population of T Cells Useful for the Treatment of Cancer [Internet]. 2019 [cited
664 2026 Jan 4].
665 https://patents.google.com/patent/US20190085063A1/en?oq=US20190085063A1. Accessed
666 4 Jan 2026

667 19. Kang CH, Kim Y, Lee DY, Choi SU, Lee HK, Park CH. c-Met-Specific Chimeric
668 Antigen Receptor T Cells Demonstrate Anti-Tumor Effect in c-Met Positive Gastric Cancer.
669 Cancers. Multidisciplinary Digital Publishing Institute; 2021;13:5738.
670 https://doi.org/10.3390/cancers13225738

671 20. Jiang W, Li T, Guo J, Wang J, Jia L, shi X, et al. Bispecific c-Met/PD-L1 CAR-T Cells
672 Have Enhanced Therapeutic Effects on Hepatocellular Carcinoma. Front Oncol [Internet].
673 2021 [cited 2022 June 28];11. https://www.frontiersin.org/article/10.3389/fonc.2021.546586.
674 Accessed 28 June 2022

675 21. Thayaparan T, Petrovic RM, Achkova DY, Zabinski T, Davies DM, Klampatsa A, et al.
676 CAR T-cell immunotherapy of MET-expressing malignant mesothelioma. OncoImmunology.
677 2017;6:e1363137. https://doi.org/10.1080/2162402X.2017.1363137

678 22. Rabinovich PM, Komarovskaya ME, Wrzesinski SH, Alderman JL, Budak-Alpdogan T,
679 Karpikov A, et al. Chimeric receptor mRNA transfection as a tool to generate antineoplastic
680 lymphocytes. Hum Gene Ther. 2009;20:51–61. https://doi.org/10.1089/hum.2008.068

681 23. Tlemsani C, Pongor L, Elloumi F, Girard L, Huffman KE, Roper N, et al. SCLC-
682 CellMiner: A Resource for Small Cell Lung Cancer Cell Line Genomics and Pharmacology
683 Based on Genomic Signatures. Cell Rep. 2020;33:108296.
684 https://doi.org/10.1016/j.celrep.2020.108296

685 24. Bloemberg D, Nguyen T, MacLean S, Zafer A, Gadoury C, Gurnani K, et al. A High-
686 Throughput Method for Characterizing Novel Chimeric Antigen Receptors in Jurkat Cells.
687 Mol Ther - Methods Clin Dev. 2020;16:238–54. https://doi.org/10.1016/j.omtm.2020.01.012

688 25. Rabinovich PM, Zhang J, Kerr SR, Cheng B-H, Komarovskaya M, Bersenev A, et al. A
689 versatile flow-based assay for immunocyte-mediated cytotoxicity. J Immunol Methods.
690 2019;474:112668. https://doi.org/10.1016/j.jim.2019.112668

691 26. Tchou J, Zhao Y, Levine BL, Zhang PJ, Davis MM, Melenhorst JJ, et al. Safety and
692 Efficacy of Intratumoral Injections of Chimeric Antigen Receptor (CAR) T Cells in
693 Metastatic Breast Cancer. Cancer Immunol Res. 2017;5:1152–61.
694 https://doi.org/10.1158/2326-6066.CIR-17-0189

695 27. Abramson J, Adler J, Dunger J, Evans R, Green T, Pritzel A, et al. Accurate structure
696 prediction of biomolecular interactions with AlphaFold 3. Nature. 2024;630:493–500.
697 https://doi.org/10.1038/s41586-024-07487-w

698 28. Vangone A, Bonvin AM. Contacts-based prediction of binding affinity in protein–protein
699 complexes. eLife. 2015;4:e07454. https://doi.org/10.7554/eLife.07454

700 29. Xue LC, Rodrigues JP, Kastritis PL, Bonvin AM, Vangone A. PRODIGY: a web server
701 for predicting the binding affinity of protein–protein complexes. Bioinformatics.
702 2016;32:3676–8. https://doi.org/10.1093/bioinformatics/btw514

703 30. Sahoo P, Yang X, Abler D, Maestrini D, Adhikarla V, Frankhouser D, et al.
704 Mathematical deconvolution of CAR T-cell proliferation and exhaustion from real-time
705 killing assay data. J R Soc Interface. 2020;17:20190734.
706 https://doi.org/10.1098/rsif.2019.0734

707 31. Lee L, Lim WC, Galas-Filipowicz D, Fung K, Taylor J, Patel D, et al. Limited efficacy of
708 APRIL CAR in patients with multiple myeloma indicate challenges in the use of natural
709 ligands for CAR T-cell therapy. J Immunother Cancer. 2023;11:e006699.
710 https://doi.org/10.1136/jitc-2023-006699

711 32. Lotze MT, Olejniczak SH, Skokos D. CD28 co-stimulation: novel insights and
712 applications in cancer immunotherapy. Nat Rev Immunol. 2024;24:878–95.
713 https://doi.org/10.1038/s41577-024-01061-1

714 33. Salter AI, Ivey RG, Kennedy JJ, Voillet V, Rajan A, Alderman EJ, et al.
715 Phosphoproteomic analysis of chimeric antigen receptor signaling reveals kinetic and
716 quantitative differences that affect cell function. Sci Signal. 2018;11:eaat6753.
717 https://doi.org/10.1126/scisignal.aat6753

718 34. Albelda SM. CAR T cell therapy for patients with solid tumours: key lessons to learn and
719 unlearn. Nat Rev Clin Oncol. 2024;21:47–66. https://doi.org/10.1038/s41571-023-00832-4

720 35. Monje M, Mahdi J, Majzner R, Yeom KW, Schultz LM, Richards RM, et al. Intravenous
721 and intracranial GD2-CAR T cells for H3K27M+ diffuse midline gliomas. Nature.
722 2025;637:708–15. https://doi.org/10.1038/s41586-024-08171-9

723 36. Shah PD, Huang AC, Xu X, Orlowski R, Amaravadi RK, Schuchter LM, et al. Phase I
724 Trial of Autologous RNA-electroporated cMET-directed CAR T Cells Administered
725 Intravenously in Patients with Melanoma and Breast Carcinoma. Cancer Res Commun.
726 2023;3:821–9. https://doi.org/10.1158/2767-9764.CRC-22-0486

727 37. Chen J, Qiu S, Li W, Wang K, Zhang Y, Yang H, et al. Tuning charge density of
728 chimeric antigen receptor optimizes tonic signaling and CAR-T cell fitness. Cell Res.
729 2023;33:341–54. https://doi.org/10.1038/s41422-023-00789-0

730 38. Wang Y, Buck A, Piel B, Zerefa L, Murugan N, Coherd CD, et al. Affinity fine-tuning
731 anti-CAIX CAR-T cells mitigate on-target off-tumor side effects. Mol Cancer. 2024;23:56.
732 https://doi.org/10.1186/s12943-024-01952-w

733 39. Freeman R, Shahid S, Khan AG, Mathew SC, Souness S, Burns ER, et al. Developing a
734 membrane-proximal CD33-targeting CAR T cell. J Immunother Cancer. 2024;12:e009013.
735 https://doi.org/10.1136/jitc-2024-009013

736 40. Slørdahl TS, Denayer T, Moen SH, Standal T, Børset M, Ververken C, et al. Anti-c-MET
737 Nanobody - a new potential drug in multiple myeloma treatment. Eur J Haematol.
738 2013;91:399–410. https://doi.org/10.1111/ejh.12185

739 41. Porazzi P, Nason S, Yang Z, Carturan A, Ghilardi G, Guruprasad P, et al. EZH1/EZH2
740 inhibition enhances adoptive T cell immunotherapy against multiple cancer models. Cancer
741 Cell. 2025;43:537-551.e7. https://doi.org/10.1016/j.ccell.2025.01.013

742 42. Barisa M, Zappa E, Muller H, Shah R, Buhl J, Draper B, et al. Functional avidity of anti-
743 B7H3 CAR-T constructs predicts antigen density thresholds for triggering effector function
744 [Internet]. 2024 [cited 2025 July 4]. https://doi.org/10.1101/2024.02.19.580939

745 43. Zhang Y, Patel RP, Kim KH, Cho H, Jo J-C, Jeong SH, et al. Safety and efficacy of a
746 novel anti-CD19 chimeric antigen receptor T cell product targeting a membrane-proximal
747 domain of CD19 with fast on- and off-rates against non-Hodgkin lymphoma: a first-in-human
748 study. Mol Cancer. 2023;22:200. https://doi.org/10.1186/s12943-023-01886-9

749 44. Alabanza L, Pegues M, Geldres C, Shi V, Wiltzius JJW, Sievers SA, et al. Function of
750 Novel Anti-CD19 Chimeric Antigen Receptors with Human Variable Regions Is Affected by
751 Hinge and Transmembrane Domains. Mol Ther J Am Soc Gene Ther. 2017;25:2452–65.
752 https://doi.org/10.1016/j.ymthe.2017.07.013

753 45. Hamieh M, Mansilla-Soto J, Rivière I, Sadelain M. Programming CAR T Cell Tumor
754 Recognition: Tuned Antigen Sensing and Logic Gating. Cancer Discov. 2023;13:829–43.
755 https://doi.org/10.1158/2159-8290.CD-23-0101

756 46. Shah PD, Huang ACC, Xu X, Zhang PJ, Orlowski R, Matlawski T, et al. Phase I trial of
757 autologous cMET-directed CAR-t cells administered intravenously in patients with
758 melanoma & breast carcinoma. J Clin Oncol. Wolters Kluwer; 2020;38:10035–10035.
759 https://doi.org/10.1200/JCO.2020.38.15_suppl.10035

760 47. Chiriaco C, Donini C, Cortese M, Ughetto S, Modica C, Martinelli I, et al. Efficacy of
761 CAR-T immunotherapy in MET overexpressing tumors not eligible for anti-MET targeted
762 therapy. J Exp Clin Cancer Res. 2022;41:309. https://doi.org/10.1186/s13046-022-02479-y

763 48. Kong B, Kim Y, Kim EH, Suk JS, Yang Y. mRNA: A promising platform for cancer
764 immunotherapy. Adv Drug Deliv Rev. 2023;199:114993.
765 https://doi.org/10.1016/j.addr.2023.114993

766
767

768

769 **FIGURE LEGENDS**

770 **Figure 1 VHH-CAR-T with intermediate avidity showed the most potent killing.**
771 (A) Schematic diagram of VHH-CAR construct. (B) Expression level of VHH-CAR by GFP.
772 Red peak = mock electroporated T cells. (C) Avidity curve of VHH-CAR-T against MDA-MB-
773 231, with the % T cells bound to target cells at 1000 pN shown in (D). N = 4 technical
774 replicates; *P* values comparing avidity at 1000 pN were calculated using one-way ANOVA).
775 (E) AlphaFold3 modeling of VHH binding sites on MET. MET = cyan; HGFα chain = light
776 gray; HGFβ chain = dark gray; VHH1 = red; VHH2 = blue; VHH3 = orange; VHH4 = green;
777 VHH5 = brown. (F) VHH-CAR-T cytotoxicity against MDA-MB-231 (n=4 technical replicates;
778 *P* values by two-way ANOVA). (G) VHH1 and VHH2-CAR-T against A549, with tumor
779 proliferation monitored in CellCyte (n=6 technical replicates; *P* values by two-way ANOVA).
780 Data shown are mean$\pm$SD; *$P<0.05$; **$P<0.01$; ***$P<0.001$; ****$P<0.0001$.

781

782 **Figure 2: CD28 costimulatory domain conferred stronger VHH2-CAR activation.** (A)
783 Expression level of mRNA VHH2-BBz and VHH2-28z in primary human T cells. (B) Avidity
784 assay using Lumicks z-Movi, comparison between VHH2-BBz and VHH2-28z (n = 3
785 technical replicates; two-way ANOVA). (C) Comparison of MDA-MB-231 killing between
786 VHH2-BBz and VHH2-28z (n=8 technical replicates, two-way ANOVA). (D) Intracellular
787 cytokine production analyzed by flow cytometry; cells harvested 16 hours after co-culture
788 with MDA-MB-231 in the presence of 2μM of the Golgi inhibitor monensin (n = 4 technical
789 replicates, two-way ANOVA). (E) Polyfunctioinal strength index (PSI) using IsoPlexis,
790 comparison between CD8+ VHH2-BBz and CD8+ VHH2-28z 16 hours after co-culture with
791 Karpas-422. Effector cytokines (Granzyme B, IFN-γ, MIP-1a, perforin, TNF-α, TNF-β);
792 Stimulatory cytokines (GM-CSF, IL-12, IL-15, IL-2, IL-21, IL-5, IL-7, IL-8, IL-9);
793 Chemoattractive cytokines (CCL-11, IP-10, MIP-1b, RANTES); Regulatory cytokines (IL-10,
794 IL-13, IL-22, IL-4, sCD137, sCD40L, TGF-b1); Inflammatory cytokines (IL-17A, IL-17F, IL-1b,
795 IL-6, MCP-1, MCP-4). (F-I) Microwell assay using TROVO, comparing single cell killing rate

796 (F) (n=3 technical replicates; two-tailed Student's *t*-test), T cell proliferation (G) (n=2
797 donorsx3 replicates; two-tailed Student's *t*-test), and tumor killing (H) (n=2 donors x 3
798 replicates each, two-tailed Student's *t*-test). (I) Representative images used to calculate
799 data shown in (G) and (H). Each row represents one microwell monitored over 4 days. Each
800 microwell is set up with E:T =20:10. T cell = red. **P<0.05; **P<0.01; ***P:<0.001;*
801 *****P:<0.0001.*
802
803 **Figure 3: In vitro and in vivo efficacy of VHH2-CAR.** (A) MET expression in tumor cell
804 lines. Red = IgG isotype control. (B) Cytotoxicity of VHH2-CAR-T cells at different E:T ratios
805 (n=3 technical replicates; two-way ANOVA). (C) Scheme of in vivo experiment using the
806 LM2 tumor model. (D) BLI of tumor growth in vivo. PBS = 3 animals; Mock T = 2 animals;
807 VHH2-CAR-T = 3 animals. *P* values were calculated using two-way ANOVA. (E) MET IHC,
808 10x objective on the left and 20x objective on the right. The boxed regions were magnified
809 and shown on the right. The bar graph represents quantifications of MET expression. *P*-
810 value was calculated by two-tailed Student's *t*-test. (F) CD3 IHC, 20x objective. **P<0.05;*
811 ***P<0.01; ***P<0.001; ****P<0.0001.*
812
813 **Figure 4: Antigen threshold for VHH2-CAR.** (A) mRNA and western blot of MET
814 expression levels in a series of small cell lung cancer cell lines. The mRNA data comes from
815 CellMiner[23]. (B and C) MET expression by flow cytometry and cytotoxicity in NCI-H1341.
816 N= 3 technical replicates in the cytotoxicity assay; *P* values from two-way ANOVA. (D-E)
817 MET expression by flow cytometry and cytotoxicity in NCI-H146. N= 3 technical replicates; *P*
818 values calculated using two-way ANOVA. (F) Histogram of MET expression levels in
819 different cell lines. (G) Cytotoxicity of VHH2-CARs against the same cell lines as in (E). N= 3
820 technical replicates; *P* values calculated using two-tailed Student's *t*-test. **P<0.05; **P<0.01;*
821 ****P<0.001; ****P<0.0001.*
822

823 **Figure 5: VHH-CARs showed low tonic signaling.** (A) Experimental design of CAR-Jurkat
824 assay. (B) Comparison of CD69 expression in CAR-Jurkat cells with varying levels of
825 antigen stimulation. (C) Comparison of CD69 expression in primary human T cells
826 electroporated to express CARs. E:T ratio was 1:1, and co-culture was incubated for 16
827 hours before staining for flow cytometry. (D-E) Cytotoxicity comparison between VHH2,
828 scFv1, and scFv2 using two different cell lines with different MET expression levels. (F)
829 Electrostatic surface charge of MET binders. Modeling was performed using PyMol. Blue =
830 more basic/positive charge; red = more acidic/negative charge; white = neutral. In
831 experiments shown in B-E, n=3 technical replicates, and *P* values were calculated with two-
832 way ANOVA. *$^{*}P<0.05$; $^{**}P<0.01$; $^{***}P<0.001$; $^{****}P<0.0001$.*
833
834 **Figure 6: Avidity and kinetics comparisons of CARs.** (A) Different binding epitopes
835 predicted by AlphaFold3 for VHH2, scFv1, and scFv2. (B) Expression of compared CARs.
836 (C) Avidity measurement by Lumicks z-Movi using MDA-MB-231 as target cells. N = 3
837 technical replicates, with *P* values from two-tailed Student's *t*-test. (D) Avidity measurement
838 against the 786-O cell line. N = 4-5 technical replicates; *P* values from two-tailed Student's *t*-
839 test. (E) Intracellular cytokine production by flow cytometry. Cells were stained before and
840 16-hours after stimulation by Karpas-422. N=3 technical replicates; *P* values from two-way
841 ANOVA. (F) Polyfunctional strength index by IsoPlexis. Effector cytokines (Granzyme B,
842 IFN-γ, MIP-1a, perforin, TNF-α, TNF-β); Stimulatory cytokines (GM-CSF, IL-12, IL-15, IL-2,
843 IL-21, IL-5, IL-7, IL-8, IL-9); Chemoattractive cytokines (CCL-11, IP-10, MIP-1b, RANTES);
844 Regulatory cytokines (IL-10, IL-13, IL-22, IL-4, sCD137, sCD40L, TGF-b1); Inflammatory
845 cytokines (IL-17A, IL-17F, IL-1b, IL-6, MCP-1, MCP-4). (G-I) Hydrogel-based microwell co-
846 culture assay by TROVO, showing single cell killing rate (G, 1:10 E:T), killing (H, 20:10 E:T),
847 and T cell proliferation (I, 20:10 E:T). N=3 technical replicates; *P* values using two-tailed
848 Student's *t*-test. (J) Representative images of microwell co-culture at 20:10 E:T. Each row
849 represents one microwell monitored over time. *$^{*}P<0.05$; $^{**}P<0.01$; $^{***}P<0.001$;
850 $^{****}P<0.0001$.*

851

852 **Figure 7: In vivo comparison between scFv2 and VHH2-CAR**. (A) Experimental design of
853 in vivo efficacy. (B) Kaplan-Meier survival curve using a predefined tumor burden threshold
854 of $1x10^9$ photons/sec as the survival endpoint for analysis purposes. *P*-value shown for
855 VHH2-CAR versus scFv2-CAR comparison. (C) Tumor growth curve by BLI imaging. Each
856 group = 7 mice; each line = 1 mouse. (D) Representative images of BLI.

857

858 **SUPPLEMENTAL FIGURES:**

859 **Supplemental figure 1: mRNA CAR manufacturing through electroporation.** (A) mRNA
860 CAR design. (B) RNA gel showing examples of successful mRNA synthesis and poly(A) tail
861 incorporation. (C) CAR expression was dose-dependent as shown by GFP. (D) Time course
862 of GFP decay after mRNA electroporation in T cells.

863

864 **Supplemental figure 2: Intracellular cytokine assessment.** (A) Gating strategy. (B)
865 Example flow cytometry plot of cytokine production.

866

867 **Supplemental figure 3: Lack of significant exhaustion marker expression in VHH2-28z.**
868 (A) Representative flow cytometry plot of PD-1 versus TIM3 and PD-1 versus LAG3
869 expression. CAR-T cells were co-cultured with Karpas-422 for 48 hours before harvesting for
870 flow cytometry. (B) Comparison of PD-1 and LAG3 expression, and PD-1/TIM3
871 coexpression between mock T, VHH2-28z, and VHH2-BBz T cells. N=3 technical replicates;
872 *P* values from two-way ANOVA. **P<0.05; **P<0.01; ***P<0.001; ****P:<0.0001.*

873

874 **Supplemental Figure 4: Karpas-422 cell line with MET and CD19 expression.** (A) Flow
875 cytometry demonstrating expression of both antigens. Red curve = IgG isotype control. (B)
876 Confirmation of cytotoxicity of different MET CAR-T cells and CD19-CAR-T cells against
877 Karpas-422. N = 3 technical replicates, with *P* values calculated from two-tailed Student's *t*-
878 test. **P<0.05; **P<0.01; ***P<0.001; ****P:<0.0001.*

879

880 **Supplemental Figure 5: Bulk cytokine secretion by ELISA between various CAR**

881 **constructs against MDA-MB-231.** Panel A shows selected effector cytokines, while panel

882 B shows selected cytokines known to mediate CAR T cell related toxicity and inflammatory

883 responses.

884

885

886

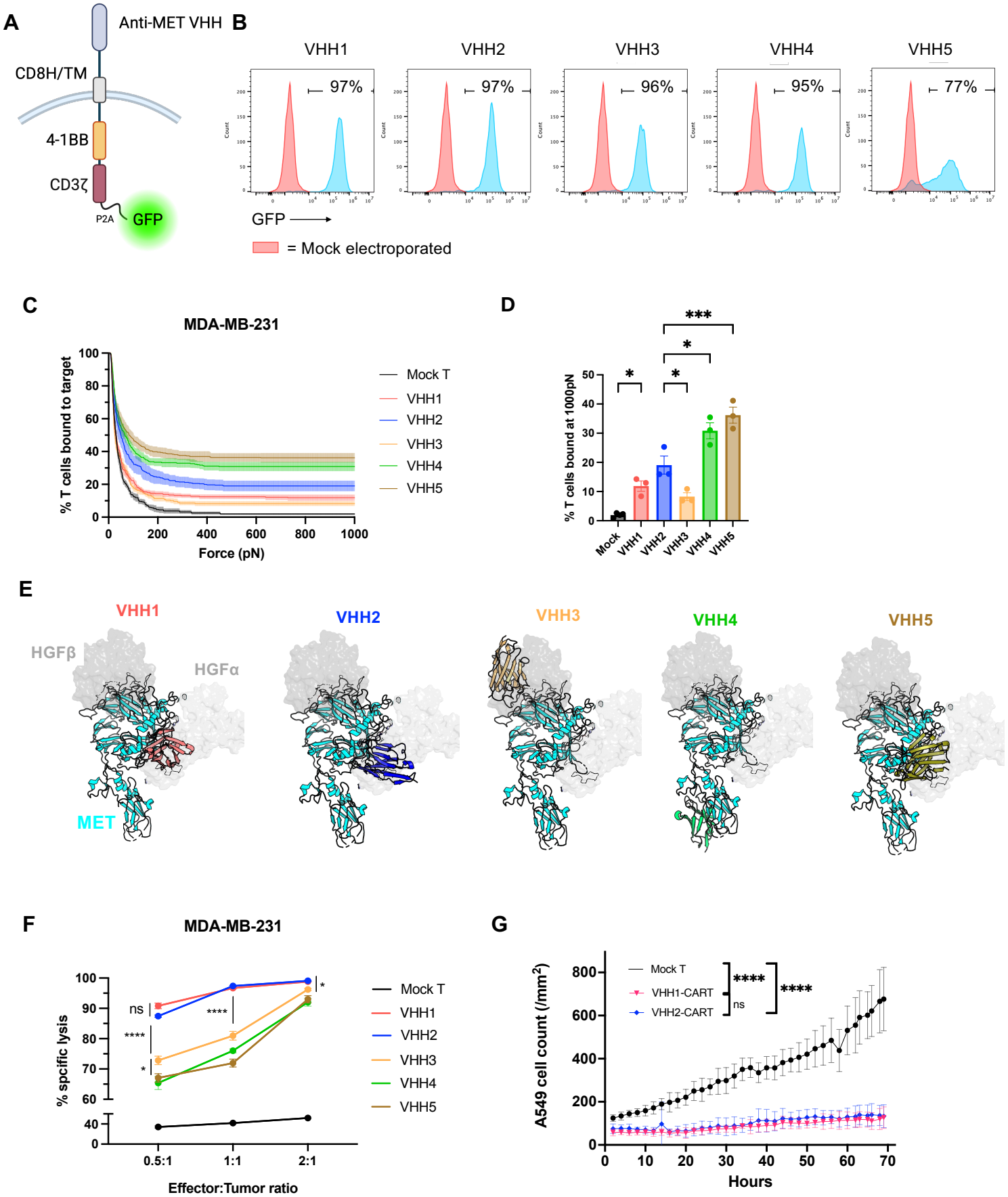

Chen, et al., Figure 1

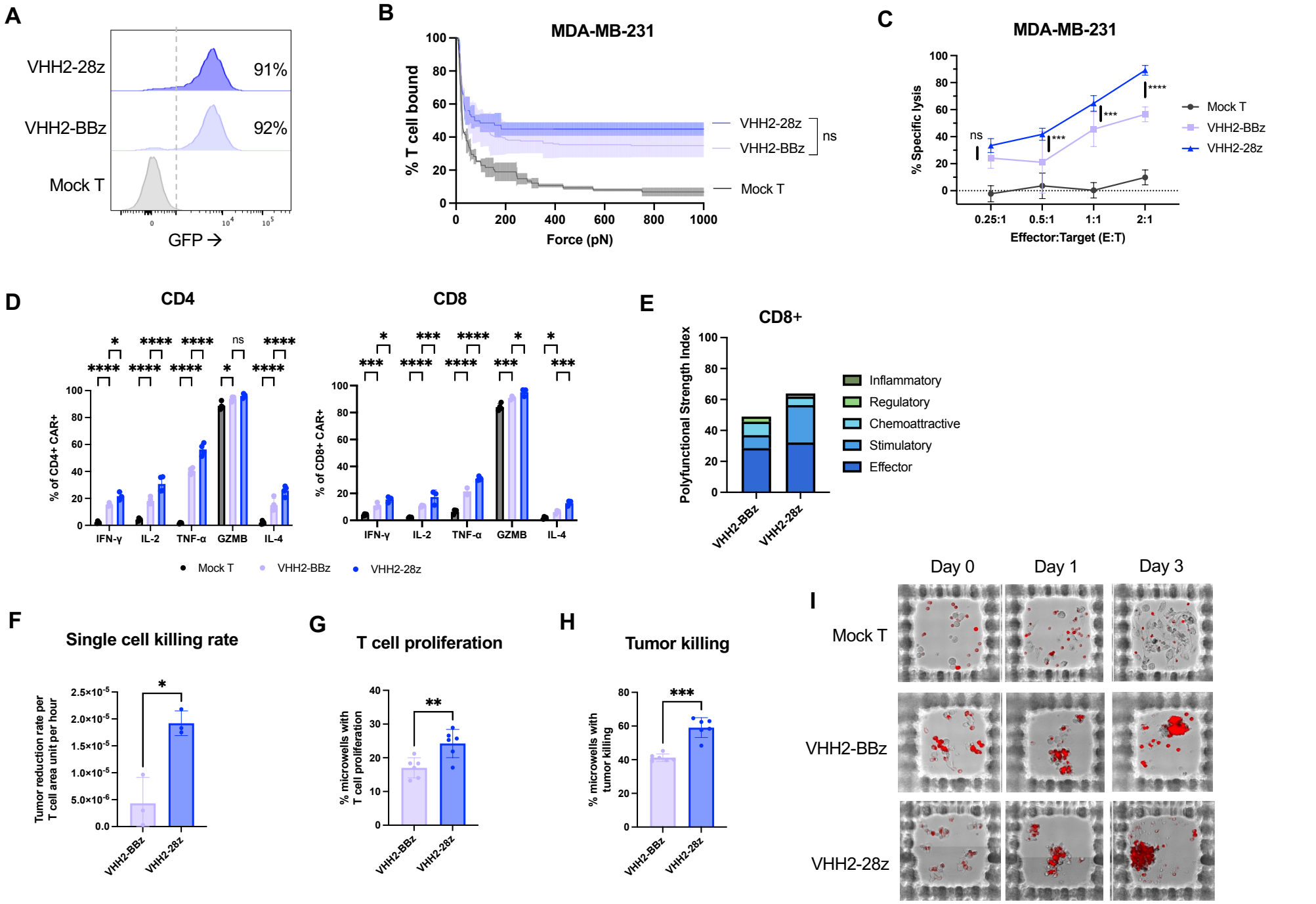

Chen, et al., Figure 2

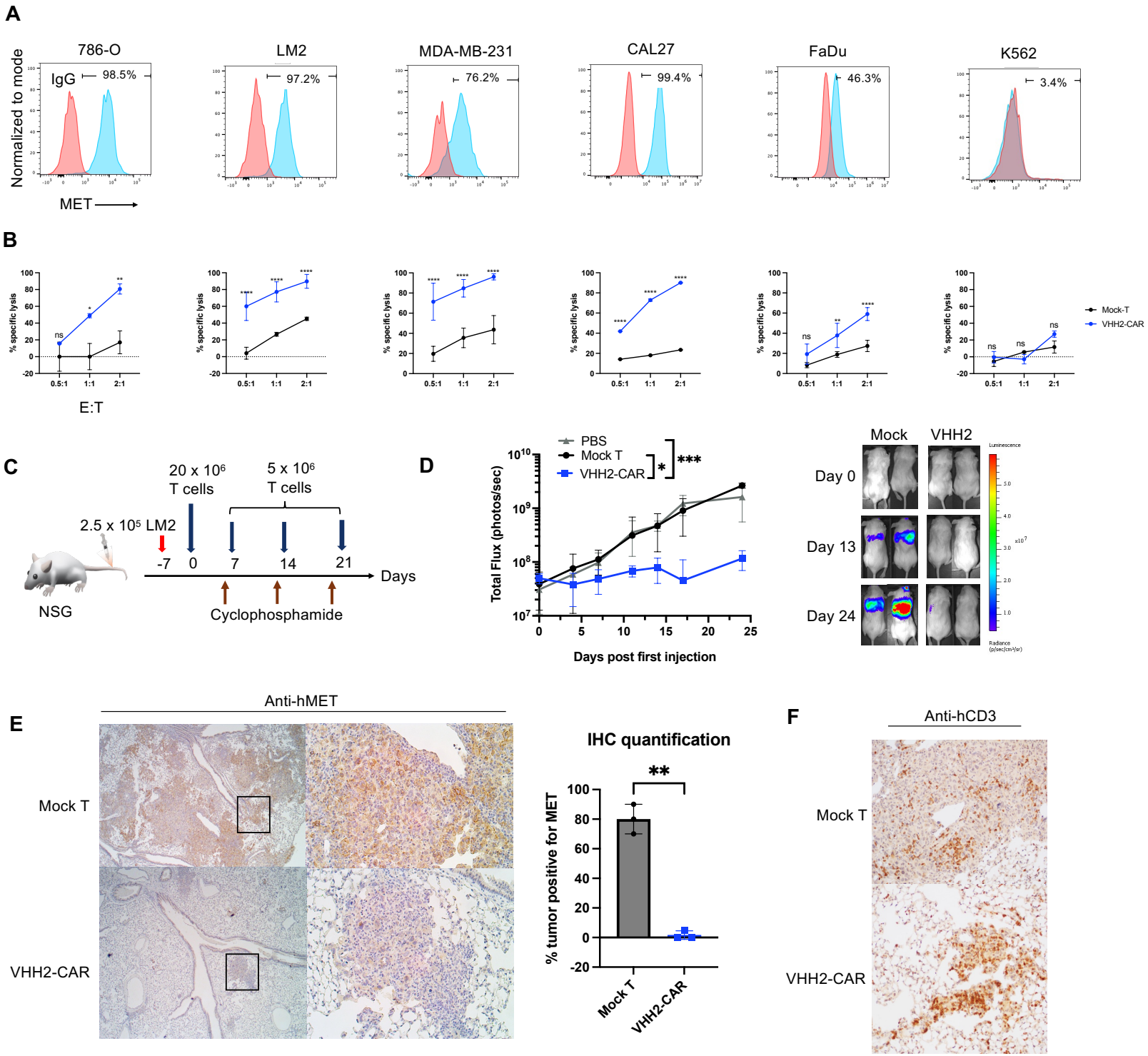

Chen, et al., Figure 3

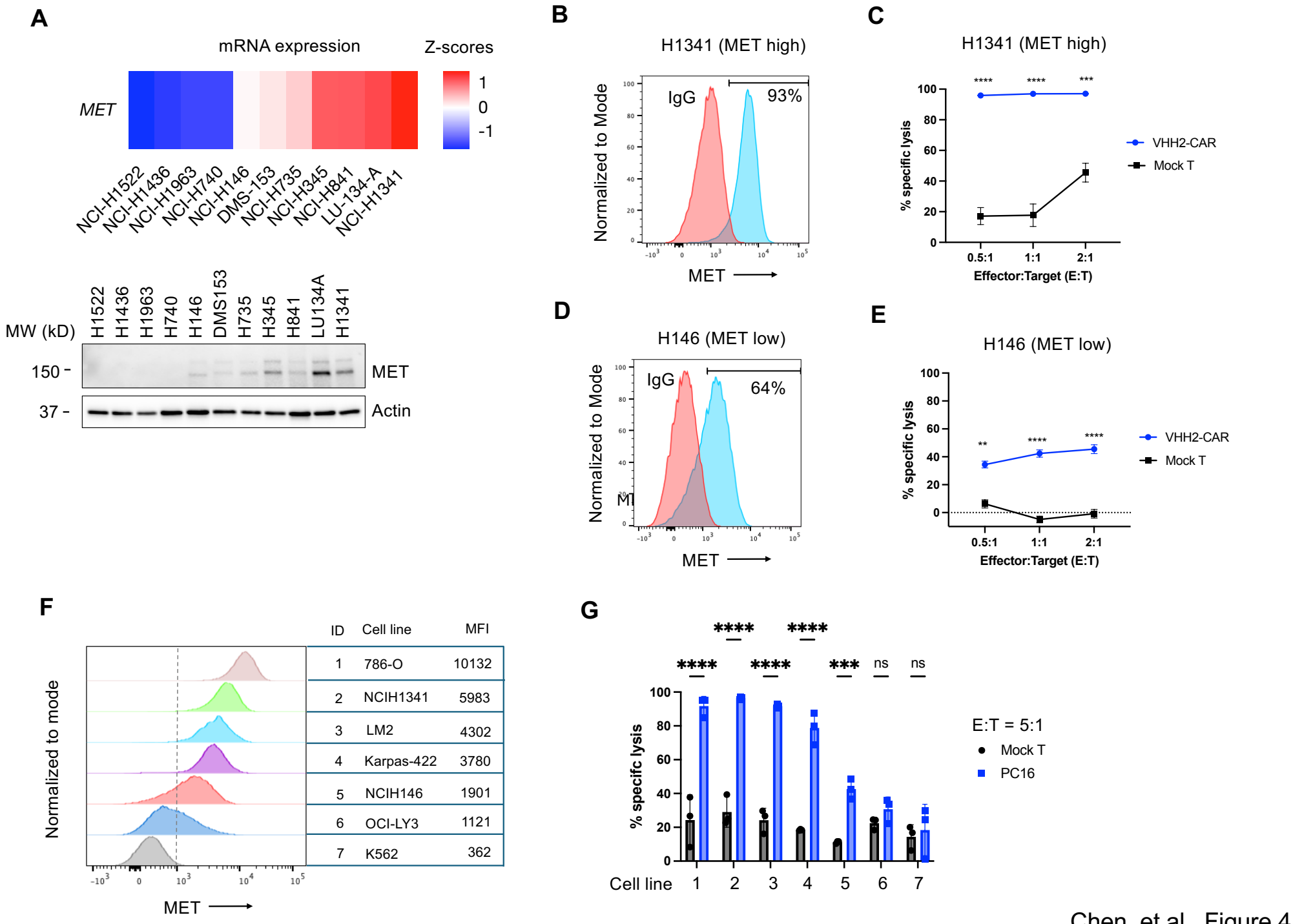

Chen, et al., Figure 4

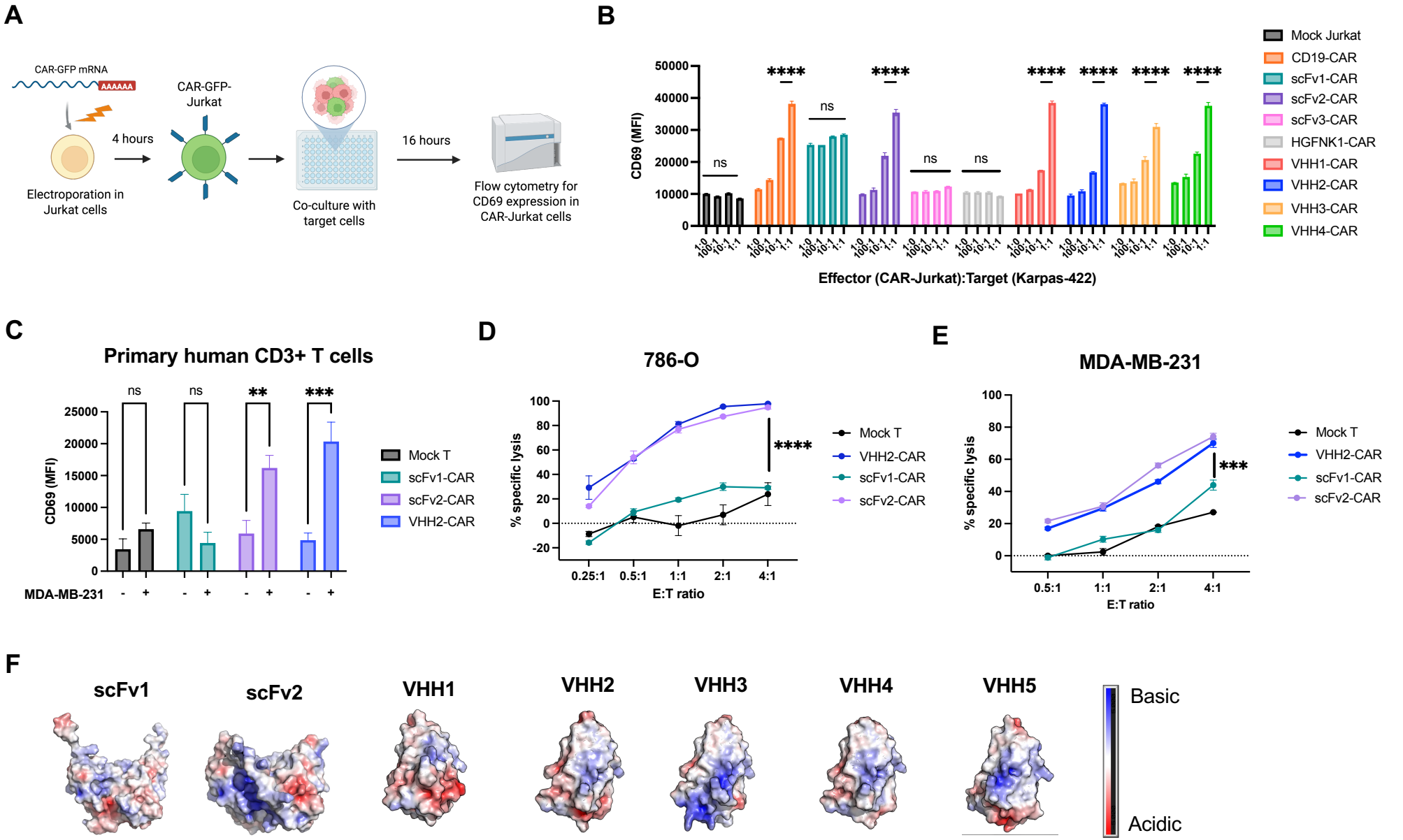

Chen, et al., Figure 5

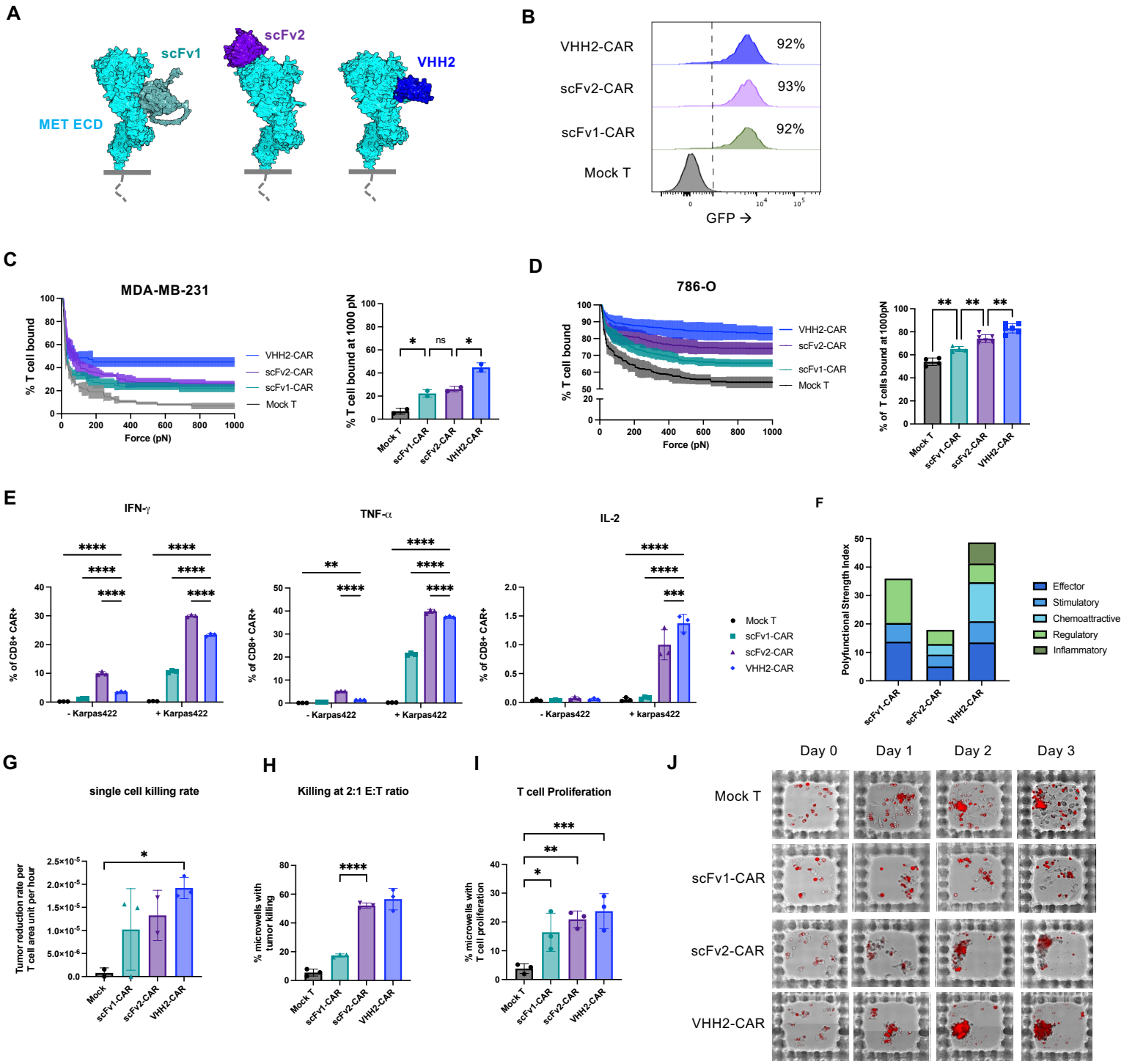

Chen, et al., Figure 6

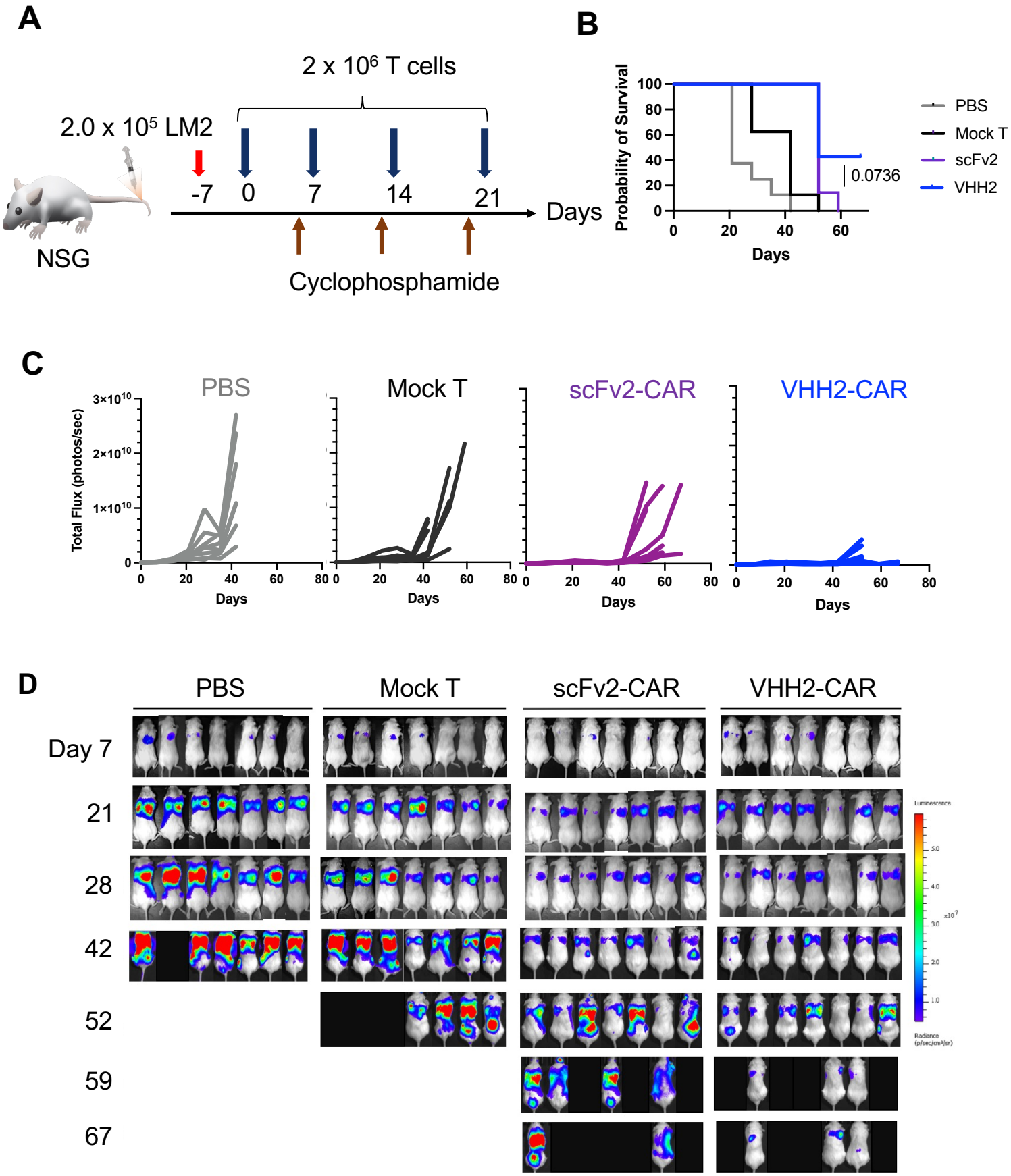

Chen, et al., Figure 7